

Catalytic Hydrodehalogenation | Very Important Paper |

The Electronic Properties of Ni(PNN) Pincer Complexes Modulate Activity in Catalytic Hydrodehalogenation Reactions

Denan Wang^[a] and James R. Gardinier*^[a]

Abstract: Three chloronickel(II) complexes of PNN- pincer ligands with pyrazolyl and diphenylphosphino donors appended to different arms of diarylamido anchors were prepared and fully characterized. The three derivatives (**1-OMe**, **1-Me**, **1-CF₃**) differ only by the identity of the *para*-aryl substituent on the pyrazolyl arm with **1-OMe** being 310 mV easier to oxidize than **1-CF₃**. All three complexes are competent catalysts for hydrode-

halogenation reactions of 1-bromooctane and a variety of aryl halides in dimethylacetamide using NaBH₄ as both base and hydride source. Comparative studies using diverse substrates showed that catalytic activity correlates with electron donor properties; **1-OMe** was superior to the other two. Deuterium labeling studies verified NaBD₄ as the deuteride source and excluded solvent-assisted radical pathways.

Introduction

Catalytic hydrodehalogenation (HDH) of organic halides is of great interest in organic synthesis and environmental pollution remediation efforts.^[1–5] Among the numerous HDH methods that have been developed,^[6–15] nickel pincer complexes have recently emerged as attractive, stable, homogeneous catalysts for such reactions.^[16–21] In 2012, the Hu group reported that “Nickamine”^[16,22] (complex **A** in Figure 1) could be used as a precatalyst for hydrodehalogenation reactions of both aryl and alkyl halides by employing diethyloxymethylsilane as reductant and sodium methoxide as base. Rettenmeier, Wadepohl and Gade found that a chiral Ni(NNN) complex, **B**, (Figure 1) can be transformed to a stable Ni(I) derivative via reaction with LiEt₃H and could be used to effect stereoselective HDH of various alkyl halides via a radical mechanism.^[18] Later this group successfully used these catalysts for HDH of aromatic halides.^[19] Norton demonstrated that this pincer complex could even effect Hydrodefluorination reactions.^[21] Pincer ligands with other donor atoms were also found to be useful for HDH reactions. Thus, Enthaler and co-workers^[17] used a (ONO)Ni^{II}PPh₃ complex, **C**, (Figure 1) in concert with either Grignard or organozinc reagents to effect HDH of aromatic and alkyl halides. The reaction was thought to proceed via the hydride from β-hydride elimination of the in-situ generated organonickel species; the expected alkyl-aryl cross-coupling products were the minor by-products of the HDH reaction. It is interesting that ligands with relatively “hard” nitrogen or oxygen donor sets allow for isolation of both

low valent nickel species, reactive nickel hydride intermediates while also supporting catalytic activity.

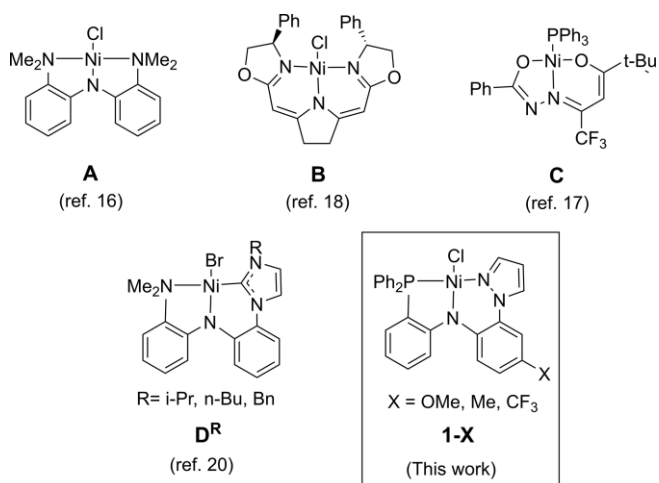


Figure 1. Representative nickel pincer precatalysts used in dehydrohalogenation reactions of organic halides.

A fundamental question prompted by the above results was whether the replacement of one (or both) of the “hard” flanking donors with groups such as carbenes or organophosphine donors would still give catalytically active species or whether the hydride or low valent nickel intermediates would be too stable to allow for catalytic turnover. A recent contribution from the Sun group^[20] addressed this question. Their carbene-containing pincer complexes (NNC)NiBr, **D^R** (Figure 1), can be converted to (NNC)NiH via reactions with sodium *tert*-butoxide as a base and triethyloxysilane as a hydride source. These (NNC)NiH can efficiently catalyze HDH reactions of various aryl and alkyl halides where the **DiPr** variant proved superior to the other two **D^R** complexes.

We sought to extend these studies to pincer complexes with organophosphine donors. Despite numerous (PNN)Ni pincer

[a] Dr. D. Wang, and Prof. J. R. Gardinier
Department of Chemistry, Marquette University,
Milwaukee, WI, USA 53201-1881
E-mail: james.gardinier@marquette.edu

Supporting information and ORCID(s) from the author(s) for this article are available on the WWW under <https://doi.org/10.1002/ejic.202000721>.

This manuscript is part of the Special Collection Pincer Chemistry and Catalysis.

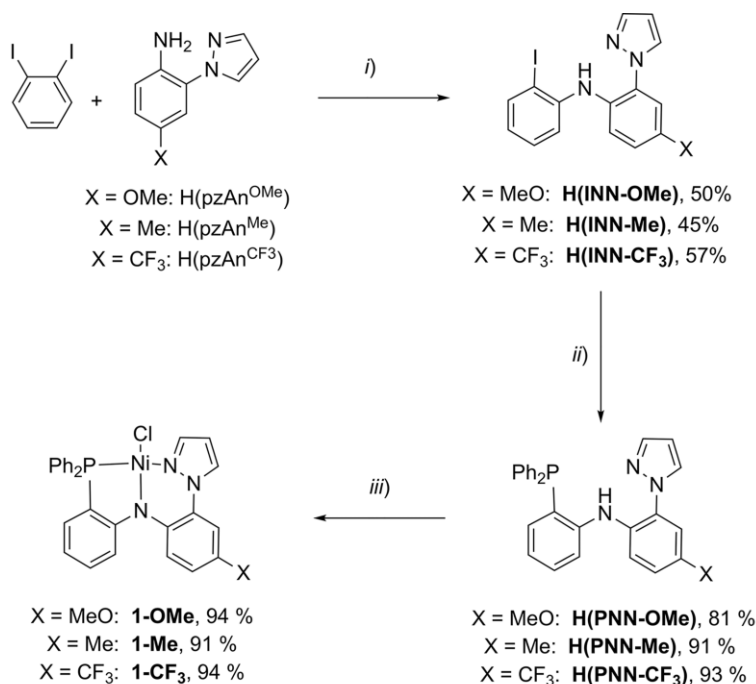
complexes being known as catalysts for a variety of reactions,^[23–29] it was fairly surprising that there were no reports of their use as catalysts for HDH reactions. Several years ago, our group introduced a PNN pincer type ligand, (*N*-2-diphenylphosphinophenyl)(*N*-2-pyrazolyl-*p*-tolyl)amine, H(PNN-Me), and showed that the hemilabile pyrazolyl arm conferred enhanced reactivity and structural adaptability to stabilize various rhodium(I/III) complexes.^[30] The modular nature of the ligand synthesis suggested a simple means to alter the electron donor strength of the ligand by varying *para*-aryl substituents. Such variants would be attractive for nickel-catalyzed HDH reactions, in that the stability of any hydride intermediates could be tuned by substitution, thereby influencing the rates of reaction. Herein, we report the preparation and properties of three new nickel(II) pincer complexes, (PNN-X)NiCl, **1-X** (X = MeO, Me, and CF₃) (Figure 1, bottom right) and disclose our initial findings regarding their ability to catalyze HDH reactions of aromatic and alkyl halides.

Results and Discussion

An overview of the syntheses of the ligands and nickel complexes is given in Scheme 1 with synthetic details provided in the Supporting Information. The CuI-catalyzed amination reaction between 1,2-diiodobenzene and the known 4-*X*-2-pyrazol-1-ylaniline, H(pzAn^X), (X = OMe, Me, or CF₃) compounds^[31] gives a mixture of mainly the desired compound along with variable amounts of unreacted H(pzAn^X) and a di-aminated product that require separation by column chromatography. Attempts to im-

prove yields of this step by using drastically different reaction times, alternative solvents, different catalysts, or adding co-catalysts have not yet been proven successful. The ensuing Pd⁰-catalyzed coupling reaction with diphenylphosphine afforded high yields of the desired H(PNN-X) ligands as air stable colorless solids. The desired nickel complexes **1-X** (X = OMe, Me, CF₃) were obtained by first mixing a CH₂Cl₂ solution of the ligand with a methanol solution of NiCl₂·6H₂O to generate a complex in-situ prior to addition of a commercial MeOH solution of NEt₄(OH) to deprotonate the ligand which is indicated by the appearance of a characteristic deep green color (vide infra) and partial precipitation. Compounds **1-X** exhibit limited solubility in MeOH which allows a facile means of separation from the soluble NEt₄Cl by-product. The compounds are soluble in THF, CH₃CN, aromatic and halocarbon solvents but are only very slightly soluble pentane, hexane, Et₂O and lower alcohols.

Solid State. Crystals suitable for single-crystal X-ray diffraction were obtained by vapor diffusion of either Et₂O (**1-Me**) or pentane (**1-OMe** and **1-CF₃**) into benzene solutions of the complexes. Views of a representative structure of **1-Me** are given in Figure 2, while other structures are provided in Figures S1 and S2. Selected bond lengths and angles are given in Table 1. Compound **1-Me** was found to crystallize as both triclinic needles (*P*1̄) and monoclinic plates (*P*2₁/*n*). The triclinic polymorph has one molecule while the monoclinic form contains two molecules in the asymmetric unit. The former is slightly more dense (1.48 g/cm³) than the latter (1.42 g/cm³) which may give rise to the more distorted square planar NiN₂PCl coordination geometry (τ_δ = 0.16 dominated by N12–Ni1–P1 163.5°) vs. those in the



key: i) 1.2 equiv Cs₂CO₃, 20 mol % CuI, dioxane Δ, 12 h;
 ii) 1.2 equiv. HPPH₂, 1.2 equiv NEt₃, 0.5 mol % Pd₂(dba)₃, 1 mol % Xantphos, dioxane, Δ, 16 h.
 iii) NiCl₂·6H₂O, (NEt₄)(OH), MeOH:CH₂Cl₂, 3 h, 295 K.

Scheme 1. Synthesis of pincer ligands and their chloronickel(II) complexes.

monoclinic form ($\tau\delta = 0.11$ (Ni1), 0.05(Ni2)). Despite the angular differences, the bond lengths about nickel in each form are quite similar. The greatest deviation occurs in the Ni1–P1 distance where the more distorted complex has a slightly longer bond (2.142 Å) than the average (2.130 Å) found in the monoclinic case. The next biggest difference occurs in the Ni1–Cl1 distance: the triclinic form measures 2.181 Å, slightly smaller than the average in the monoclinic form 2.185 Å. The Ni1–Cl1 distances are at the longer end while the Ni1–P1 distances are at the shorter end of the ranges found in other (PNN)NiCl^[26,28,29] or (PNP)NiCl^[32,33,41] complexes. In **1-Me**, the five-membered NC₂Ni chelate ring adopts an envelope conformation (fold angles = 16.3° for *P* $\bar{1}$, 11.0° and 20.1° for rings involving Ni1 and N1a, respectively, in the monoclinic form) and the six-membered NC₂N₂Ni chelate ring adopts a half-boat conformation to give an overall structure that distinguishes the phenyl rings of the PPh₂ group (Figure 2, right), with a pseudo-axial ring (type A) being closer to the toluidinyl ring than the pseudoequatorial ring (type B). In most respects, the structure of **1-OMe** is similar to those of **1-Me** with nearly identical square planar ($\tau_8 = 0.08$) coordination geometry and bond lengths about the PN₂NiCl kernel. The envelope fold angle in **1-OMe** is more severe (28.0°), which is likely influenced by crystal packing as indicated by the polymorphs of **1-Me**. The short C4–O1 bond of the anisidine unit (1.375(2) Å) in **1-OMe** does not impart any significant changes in C–C or C–N bond lengths in the aromatic ring from those displayed by **1-Me**. On the other hand, the structure of **1-CF₃** displays significantly shorter Ni1–Cl1 (2.17 vs. 2.18 Å), Ni1–P1 (2.12 vs. 2.13 Å) and N1–C1 (1.36 vs. 1.40 Å) bonds than the other two derivatives. Additionally, the Ni1–N1 distance of 1.91 Å is longer than 1.90 Å for **1-OMe**, and 1.89 Å (avg.) for **1-Me**. These trends may be explained if the inductive effect of the CF₃ group weakens the Ni–N_{amido} bond, rendering the metal more electrophilic which is then compensated for by shortening bonds with more polarizable P and Cl atoms. The Ni1–N12 (Ni–N_{pz}) distance of 1.94 Å is statistically identical to the other compounds in the series, which is in line with the observation that metal–nitrogen (pyrazolyl) bonds are generally more sensitive to oxidation and spin state changes than to inductive effects.^[34–37]

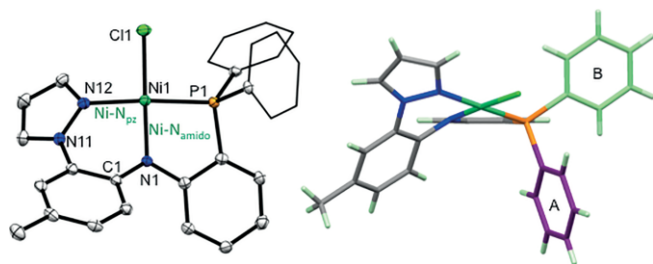


Figure 2. Left: structure of (PNN–Me)NiCl (**1-Me**, *P* $\bar{1}$ form) with partial atom labelling. Hydrogens and some phenyl carbon ellipsoids were removed for clarity; right: view parallel with the C₆H₄ moiety showing the envelope conformation of the C₂NPNi chelate ring and the distinguishable phosphino phenyl groups (A and B).

Solution. The solution structures of the three **1-X** compounds elucidated by NMR methods match expectations based on the solid-state structures. First, each ³¹P NMR spectrum contains a

Table 1. Selected bond lengths [Å] and angles (°) for (PNN–OMe)NiCl (**1-OMe**), two forms of (PNN–Me)NiCl (**1-Me**), and for (PNN–CF₃)NiCl (**1-CF₃**).

Distances[Å]	1-OMe	1-Me (<i>P</i> $\bar{1}$)	1-Me (<i>P</i> ₂ , <i>n</i>) ^[a]	1-CF₃
Ni1–Cl1	2.1825(4)	2.1808(5)	2.1854(8), 2.1855(8)	2.1718(10)
Ni1a–Cl1a			2.1855(8)	
Ni1–P1	2.1285(4)	2.1421(5)	2.1271(8), 2.1343(8)	2.1226(9)
Ni1a–P1a			2.1343(8)	
Ni1–N1	1.8992(13)	1.8895(15)	1.894(2), 1.887(2)	1.912(3)
Ni1a–N1a			1.887(2)	
Ni1–N12	1.9412(13)	1.9306(16)	1.943(2), 1.923(2)	1.941(3)
Ni1a–N12a			1.923(2)	
Angles(°)				
Cl1–Ni1–N1	176.64(4)	173.37(5)	175.36(8), 177.43(8)	175.97(8)
Cl1a–Ni1a–N1a			175.36(8)	
N12–Ni1–P1	172.52(4)	163.50(5)	169.38(7), 176.02(8)	172.44(8)
N12a–Ni1a–P1a			169.38(7)	
Cl1–Ni1–N12	93.62(4)	92.04(5)	92.50(7), 91.83(7)	93.80(8)
Cl1a–Ni1a–N12a			92.50(7)	
Cl1–Ni1–P1	93.103(17)	92.74(2)	89.73(3), 91.18(3)	91.78(4)
Cl1a–Ni1a–P1a			89.73(3)	
N1–Ni1–N12	89.58(6)	90.14(7)	91.96(10), 90.71(10)	89.86(11)
N1a–Ni1a–N12a			91.96(10)	
N1–Ni1–P1	83.76(4)	86.89(5)	86.11(7), 86.30(8)	84.72(8)
N1a–Ni1a–P1a			86.11(7)	

[a] Two molecules in asymmetric unit.

single resonance near $\delta_p = 30$ ppm that is significantly shifted downfield from the resonance for the appropriate free H(PNN–X) ligand ($\delta_p = -19.5$, -18.3 , and -16.5 ppm for X = OMe, Me, and CF₃, respectively) due to binding the nickel center. A combination of 2D NMR techniques (COSY, HMQC, HMBC) was used to unravel the rather complex ¹H and ¹³C NMR spectra (see Supporting information). The complexity arises both due to detectible ¹J to ⁴J coupling of ¹H and ¹³C nuclei with the ³¹P nucleus and because of the two sets of multiplet resonances for distinguishable phenylphosphino groups (types A and B, as in the right of Figure 2) that overlap and sometimes mask other resonances. A few points are worthy of mention regarding the NMR analysis. First, in the ¹H NMR spectra, the resonances for pyrazolyl hydrogen atom are readily identified at $\delta_H = 8.1$ (H₅), 8.0 (H₃) and 6.6 (H₄) ppm. The assignment of the latter is straightforward due its characteristic chemical shift, but the former two are tentative (vide infra), being based on both different ¹³C resonance multiplicities and ¹H–¹³C HMQC cross peaks with corresponding resonances near $\delta_C = 128.6$ (³J_{C–P} doublet, C₃) and 143.0 (singlet, C₅) ppm. Of the aromatic resonances, those of the PPh₂ group are the least electron rich and appear most downfield. Of these, the resonances for *ortho*-hydrogens appear as two doublet-of-doublets (³J_{H–P} ca. 12 Hz, ³J_{HH} ca. 8 Hz) near 7.97 and 7.87 ppm; the assignment to type B and A rings, respectively, was arbitrary and could be reversed. Their relationship to the corresponding *para*- and *meta*-hydrogens (as well as to particular *ipso*-carbons) was established by both ¹H–¹H COSY, HMQC, and HMBC experiments. The resonances for the three ring hydrogens of the pyrazolyl-aniline group are readily identified by their characteristic multiplicities in the $\delta_H = 6.7$ to 7.4 ppm region. For **1-OMe** and **1-Me**, the ¹³C NMR resonances of this group are distinguished because they are too remote to display ¹³C–³¹P coupling. For **1-CF₃**, the CF₃ and C₃–

C₄-, and C₅ nuclei of the aromatic aniline ring give characteristic quartet resonances due to ¹³C-¹⁹F coupling. Finally, the 2-phosphinoaniline group is the most electron rich aromatic ring and the ¹H corresponding resonances are generally furthest upfield, below about δ_H = 7.05 ppm, with the H₃- (*ortho*- to N) multiplet resonance near δ_H = 6.58 ppm being the most distinguishable. Similarly, in the ¹³C NMR spectrum the associated C₃- doublet resonance is uniquely upfield (δ_C = 119 ppm) while that for the C₂-ring (4° center, *ipso*-N) is the most downfield aromatic doublet resonance at ca. δ_C = 163 ppm. Interestingly, the C₆ ring nuclei (*ortho*- to P) that was expected to appear as a doublet with ²J_{C-P} coupling ca. 25 Hz (similar to the C₂- resonance) appears as a singlet. Its identity was verified by both HMQC and the strong three-bond HMBC cross peak with the H₄- resonance. Thus, assignments based on the magnitude of J_{C-P} coupling, such as those for the H(C)_{3/5} nuclei above, are tenuous and could be reversed.

The electronic properties of the three **1-X** compounds were studied by electronic absorption spectroscopy, electrochemistry (square-wave and cyclic voltammetry) and by computational methods (DFT and TD-DFT). A summary of calculated and experimental properties is given in Table 2. It is useful to first describe frontier orbitals of the complexes to facilitate discussion of electronic properties. The frontier orbitals of **1-Me** and **1-CF₃** are nearly identical to **1-OMe** (except for relative energies), so only those of the latter will be discussed. The frontier orbitals of **1-OMe** calculated at the M06/def2-SV(P) level are provided in Figure 3. Full computational details including more complete diagrams for the series of **1-X** are provided in the supporting information (Figures S23–S25). As indicated in Figure 3, the HOMO of **1-OMe** is mainly a pincer ligand π-orbital mixed in a π* manner with a minor contribution from nickel's 3d_{yz} orbital. The 3d_{yz} orbital is mainly involved in dπ–pπ interactions with the chloride p_z orbitals where the π* combination found in HOMO(–2) and the corresponding π-bonding component comprises HOMO(–1) and the corresponding π-bonding component comprises HOMO(–11 and –13), Figure S23. The HOMO(–1) is mainly nickel's 3d_{z²} orbital involved in σ*-interactions with P and anilino-N orbitals with minor contributions from the ligand π system and chloride p_y orbital. The LUMO has the Ni 3d_{x²–y²} involved in a classical σ* interaction with ligand group orbitals, while the LUMO (+N) (N = 1–7) are exclusively ligand based π* orbitals.

Table 2. Summary of experimental and calculated (M06/def2-SV(P)/PCM(CH₂Cl₂)) properties for **1-X** (X = OMe, Me, CF₃).

Compound	E' _{1+/1} , V ^[a]	UV/Vis (CH ₂ Cl ₂) λ _{max} , nm, (ε, M ⁻¹ cm ⁻¹)
1-OMe exp.	+0.51 ^[b]	660 (930), 480 sh (1100), 429 (3200), 334 (8340)
(Calcd)	+0.52	820 (175), 604 (540), 391, (7940), 339 (9710)
1-Me exp.	+0.59 ^[b]	656 (910), 478 sh (1100), 419 (3100), 334 (9040)
(Calcd)	+0.61	832 (154), 604 (480), 391, (7900), 339 (11200)
1-CF₃ exp.	+0.82 ^[b]	630 (780), 470 (830), 395 (3100), 355 (7700)
(Calcd)	+0.91	841 sh(140), 606 (425), 373 (8032), 328 (14900)

[a] V vs. Ag/AgCl. [b] In CH₂Cl₂, NBu₄PF₆ as supporting electrolyte, average of potentials acquired at scan rates of 100, 200, 300, and 400 mV/s.

The three **1-X** complexes exhibit reversible oxidations (Figure 4) whose E' _{(1-X)+/(1-X)} reduction potentials scale linearly with the electron donating nature of the *para*-anilino substituent as quantified using the substituent's Hammett σ_{para}

(PNN-OMe)NiCl M06/def2SVP/PCM(CH₂Cl₂)

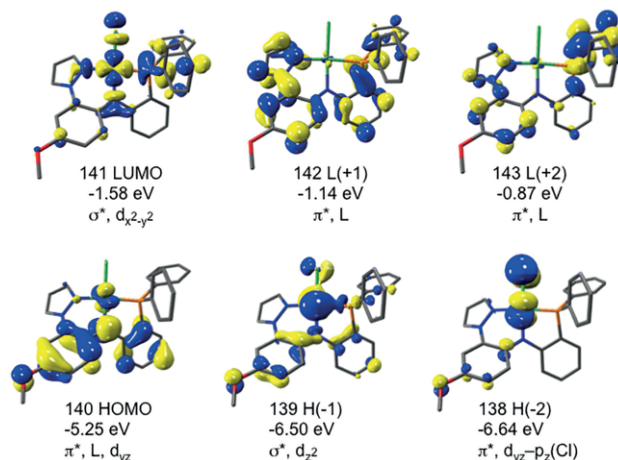


Figure 3. Selected frontier orbitals for **1-OMe** calculated at the M06/def2-SV(P)/PCM(CH₂Cl₂) level of theory with orbital number, energies, and main contributions shown.

parameter^[38] (Figure S18). That is, **1-OMe** is easier to oxidize (E' _{(1-OMe)+/(1-OMe)} = 0.51 V vs. Ag/AgCl, σ_{para} = –0.27) than **1-CF₃** (E' _{(1-CF₃)+/(1-CF₃)} = 0.82 V vs. Ag/AgCl, σ_{para} = +0.54). It is also noted that the calculated oxidation potentials give excellent agreement with the experimental values, providing another measure (along with excellent agreement of bond lengths) to validate our choice of using this DFT model. Finally, as can be elucidated by inspection of the HOMO in **1-OMe** or of the Mulliken spin-densities of atoms in (**1-OMe**)⁺ (Figure 4, right), the oxidation event of **1-OMe** is mainly (88 %) ligand-based such that (**1-OMe**)⁺ is best described as Ni^{II}-L⁺, rather than (Ni^{III}-L)⁺.

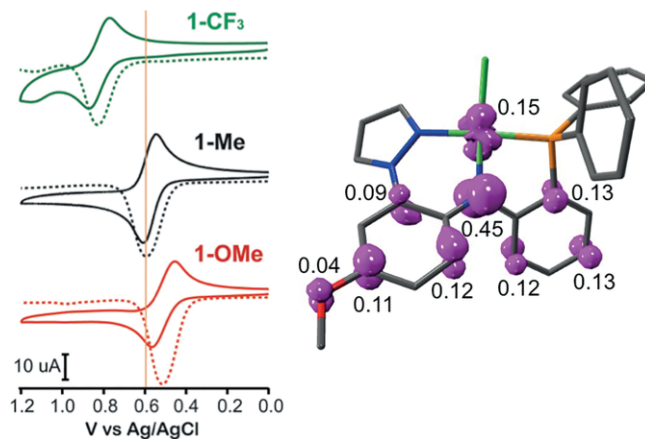


Figure 4. Left: cyclic voltammograms obtained for **1-X** (X = OMe, Me, CF₃) at a scan rate of 200 mV/s in CH₂Cl₂ with NBu₄PF₆ as a supporting electrolyte; right: Mulliken spin densities and isosurface (isovalue 0.05) of (**1-OMe**)⁺.

An overlay of the UV/Visible spectra of the three **1-X** compounds is shown in Figure 5 while data are summarized in Table 2. Details regarding calculated (time-dependent density functional theory, TD-DFT) spectra along with calculated spectra are provided in the Supporting information (Figures S26–S27). The lowest energy and least intense (ε ca. 800 to 1000 M⁻¹ cm⁻¹) band in the 600 to 750 nm range gives rise to the green or green blue color of the complexes. The modest

intensity and the hypo- and hypso-chromic shifts on ligand substitution of OMe with more electron withdrawing substituents are suggestive of ligand-to-metal charge transfer (LMCT) character.^[34] This assertion is also obtained via analysis of TD-DFT results (Tables S5 – S7), albeit not straightforwardly. The lowest energy experimental band is resolved by TD-DFT into disparate bands: a low-intensity (ϵ ca. $100 \text{ M}^{-1} \text{ cm}^{-1}$), low-energy (ca. $12,000 \text{ cm}^{-1}$, λ_{max} ca. 830 nm) component A and a more intense (ϵ ca. $400\text{--}500 \text{ M}^{-1} \text{ cm}^{-1}$), higher energy (ca. $16,500 \text{ cm}^{-1}$, λ_{max} ca. 605 nm) component B. These bands involve admixtures of HOMO(+N) \rightarrow LUMO transitions where $N = 0\text{--}2$ (component A) and $N = 3, 5$ (component B). Thus all have $d\text{--}d$ character but component A HOMO(+N) has significant contributions from pincer ligand π system and chloride p_z (and to a lesser extent p_x) orbitals whereas the HOMO(+3 and +5) of component B have substantial contributions from chloride p_x -orbitals (Figure S23) with little or no contribution from pincer ligand orbitals. As such, the energy of the component A band is more ligand dependent than that of component B. In general, transitions involving the ligand-based HOMO as the origin of a transition will experience ligand-dependent hypsochromic shifts along the series **1-OMe** to **1-CF₃**, which is exhibited by the next two higher energy bands in the 400–500 nm range of the experimental spectra. These latter two bands are due to overlapping HOMO \rightarrow LUMO (+0 and +1) transitions for the lower energy shoulder (λ_{exper} ca. 470–480 nm, λ_{TDDFT} ca. 391 nm) and to overlapping HOMO \rightarrow LUMO (+2, +3, and +4) transitions for the higher energy band (λ_{exper} ca. 395–430 nm, λ_{TDDFT} ca. 333 ± 6 nm). The more intense band (ϵ ca. $9000 \text{ M}^{-1} \text{ cm}^{-1}$) or split bands (**1-CF₃**) near λ_{exper} ca. 350 nm have MLCT character, being lowest energy for **1-CF₃** and highest for **1-OMe**. Accordingly, TD-DFT predicts these bands (λ_{TDDFT} ca. 280 ± 4 nm) to be due to mainly overlapping transitions between metal-based HOMO(–1, –2, or –5) to LUMO(+1), a pincer π^* orbital.

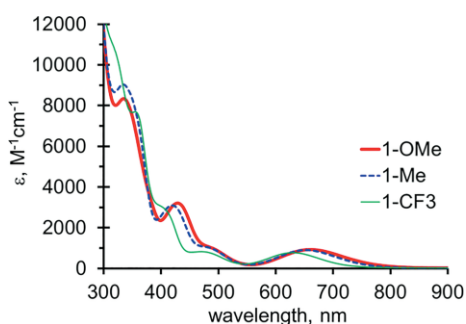


Figure 5. Overlay of the UV/visible spectra of **1-X** (X = OMe, thick solid red line; X = Me, dashed blue line; X = CF₃, thin solid green line) in CH₂Cl₂.

Catalysis. With the series of electronically diverse nickel pincer complexes in hand, their utility in hydrodehalogenation reactions was investigated. NaBH₄ was selected as the hydride source because it is conveniently handled^[39,40] and is, by far, the least expensive of the commonly used reductants. The compound 4-bromobiphenyl was chosen as an initial substrate for reaction optimization because it and its product, biphenyl, are readily available, easily-handled solids that can be reliably quantified both on the spectroscopic and synthetic scale without

significant losses due to inadvertent evaporation. A reaction time of 3 h was arbitrarily chosen for the initial survey as it was reasonably short to allow rapid screening. Fortuitously, this time period provided useful window into reactivity differences, so no further effort was made to optimize the reaction time. A summary of results from HDH reaction optimization studies is found in Table 3, with the optimized conditions found in entries 1–4. That is, all three complexes were excellent at catalyzing the HDH reaction of 4-bromobiphenyl at 8 mol-% loading, with **1-OMe** being slightly superior to the other two complexes. The yields of product decrease with lower catalyst loading (4 mol-%, entries 5–7) and the superiority of **1-OMe** vs. **1-Me** becomes evident. The **1-X** complexes all outperform simple nickel salts and the reaction does not proceed in the absence of nickel (entries 8–12). A control reaction with **1-OMe** in the presence of a drop of elemental mercury (entry 2), showed no significant reduction in efficiency suggesting that nickel colloids are not responsible for the catalytic activity. A second control (not tabulated) showed that no reaction occurred in the presence of the stable radical 2,2,6,6-tetramethylpiperidinyl-N-oxyl (TEMPO), suggesting either a radical pathway or an irreversible reaction with a non-radical intermediate. In initial temperature screenings, 80 °C was found to be the optimal reaction temperature to give a maximum yield of biphenyl during the 3 h reaction time; there was no improvement in reactions performed at 100 °C. Finally, screening different solvents (compare entries 15

Table 3. Optimization of conditions for hydrodehalogenation of 4-bromobiphenyl using NaBH₄ as a reductant.^[a]

Entry	Pre-catalyst	mol-%	solvent	[°C]	yield ^[b]
1	1-OMe	8	DMA	80	98
2	1-OMe ^[c]	8	DMA	80	96
3	1-Me	8	DMA	80	97
4	1-CF₃	8	DMA	80	89
5	1-OMe	4	DMA	80	76
6	1-Me	4	DMA	80	70
7	1-CF₃	4	DMA	80	54
8	Ni(dppe)Cl ₂	4	DMA	80	17
9	Ni(DME)Cl ₂	4	DMA	80	14
10	NiCl ₂ ·6H ₂ O	4	DMA	80	7
11	Ni(OAc) ₂	4	DMA	80	6
12	none	4	DMA	80	0
13	1-OMe	4	DMA	100	78
14	1-Me	4	DMA	100	67
15	1-Me	4	DMA	60	55
16	1-Me	4	DMA	40	25
17	1-Me	4	DMA	20	7
18	1-Me	4	DMF	60	32
19	1-OMe	8	DMF	80	76
20	1-Me	4	THF	60	33
21	1-Me	4	dioxane	60	28
22	1-Me	4	<i>i</i> PrOH	60	25
23	1-Me	4	toluene	60	0

[a] Typical conditions: 0.2 mmol of 4-bromobiphenyl (46.6 mg), 0.016 mmol of Ni catalyst (8 mol-%), NaBH₄ (15.0 mg, 0.4 mmol, 2.0 equiv.) and 2 mL dimethylacetamide (DMA) or other solvent, heat 3 h. [b] GC/MS yield, average of three experiments, error $\pm 3\%$. [c] In the presence of Hg⁰ (l).

and 18–23) showed that DMA was superior to other solvents; the insolubility of NaBH₄ being the critical factor in the lack of activity in toluene.

Next, the scope of the HDH reactions with a variety of aromatic and alkyl halides was explored, with results provided in Table 4. The conversion of halobenzenes to benzene catalyzed by **1-OMe** (under conditions optimized for bromobiphenyl above) decreased up the periodic table being quantitative for iodobenzene and zero for fluorobenzene (entries 1–4). This trend roughly parallels the expected stability of the corresponding halo radical, but biphenyl was never observed as a by-product. Substrate electronic effects were probed in HDH reactions of para-*R*-substituted bromobenzenes catalyzed by **1-OMe** (R = Ph: Table 3, entry 1; R = H, Me, OMe, CN: Table 2, entries 2, 5, 6, and 9). The yields of the dehalogenated product are suppressed for the electron releasing substituents, R = Me and MeO whereas they are quantitative for electron withdrawing CN. If one considers Hammett σ_{para} to be indicative of electron releasing capabilities of the R group, the yield for the conversion of bromobenzene (R = H) is lower than expected; a phenyl is more electron releasing than H (σ_{para} (Ph) = -0.01 vs. σ_{para} (H) = 0.00) yet the yield for R = Ph was higher than the R = H case (98 % vs. 85 % yield, respectively). Other factors such as resonance stabilization of radical species or simply redox potentials may also be (minor) contributing factors in determining conversion. Next, the electronic effects of the **1-X** catalysts were evaluated for 4-bromoanisole (Table 4, entries 6–8) and 4-bromobenzonitrile (Table 4, entries 10–12) to validate the generality of results observed for 4-bromobiphenyl (Table 3, entries 1 and 3–7) on electronically diverse substrates. All three catalysts were excellent at catalyzing the HDH reaction of the electron-poor bromobenzonitrile, with **1-CF₃** being marginally less efficient than the other two (93 % vs. quantitative conversion). With the more electron rich anisole substrate, the yield increased inversely with (pre)catalyst oxidation potential: **1-CF₃** (29 %) < **1-Me** (45 %) < **1-OMe** (55 %). Interestingly, **1-OMe** performed as well as “nickamine”, **A**, (Table 4, entries 8 and 9). Such results suggest that further modifying **1-X**, nickamine or other nickel pincer complexes with electron donor groups might be key to improving catalytic performance toward electron rich aromatics. Next di-halogenated arenes were examined. With **1-OMe** as a catalyst, the substrates 1-bromo-2-fluorobenzene and 1-bromo-2-fluoro-4-trifluoromethylbenzene (Table 4, entries 12 and 13) underwent exclusive debromination with the more electron-deficient tri-substituted derivative reacting faster, giving quantitative conversion with half the catalytic loading and only 1 h heating. In accord with the increased activity with number of electron withdrawing substituents, *ortho*-dichlorobenzene was a more receptive substrate (27 % total (ca. 26:1 ClC₆H₅:C₆H₆), Table 4 entry 14) than the meta-dichlorobenzene (19 % total (ca. 18:1 ClC₆H₅:C₆H₆), Table 4 entry 15) which, in turn, was better than chlorobenzene (8 %, entry 3). Finally, it was found that **1-OMe** was an excellent catalyst for HDH reactions with a polyaromatic bromides (entries 16–18), heterocyclic 2-bromopyridine (entry 19), and was especially potent for transformations of benzyl bromide and 1-bromooctane (entries 20 and 21).

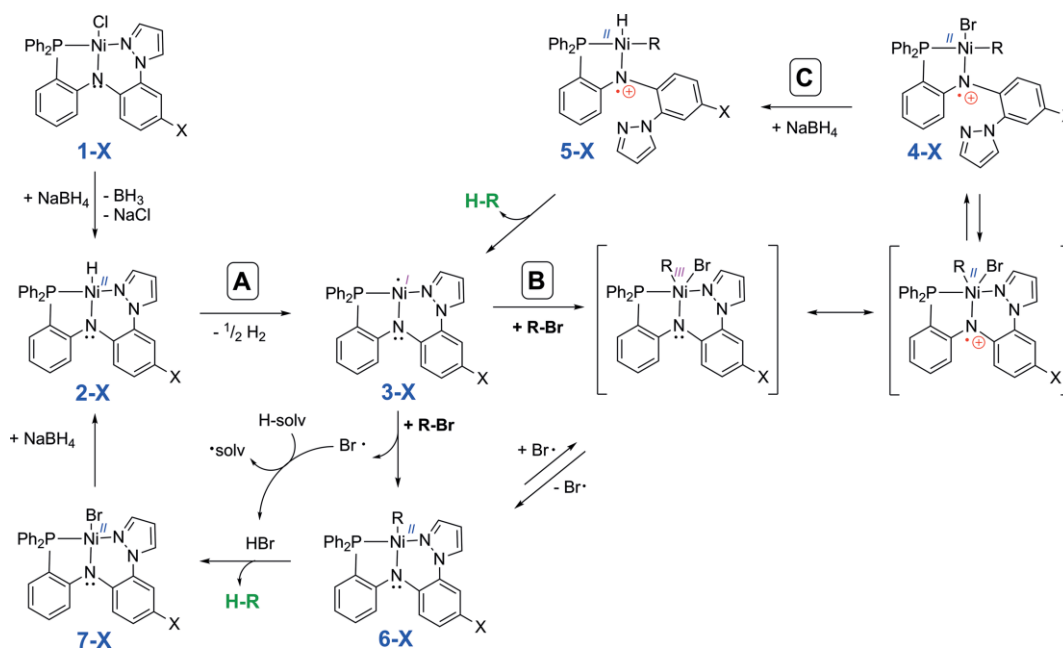
Table 4. Summary of catalytic hydrodehalogenation reactions of aryl and alkyl halides.^[a]

Entry	R	Y	X	pre-catalyst	Special Conditions	[%] yield ^[b]
1	H	H	I	1-OMe		99
2	H	H	Br	1-OMe		85
3	H	H	Cl	1-OMe		8
4	H	H	F	1-OMe		0
5	Me	H	Br	1-OMe		61
6	MeO	H	Br	1-OMe		55
7	MeO	H	Br	1-Me		45
8	MeO	H	Br	1-CF₃		29
9	MeO	H	Br	A		53
10	CN	H	Br	1-OMe		97
11	CN	H	Br	1-Me		99
12	CN	H	Br	1-CF₃		93
13	H	F	Br	1-OMe		94
14	CF ₃	F	Br	1-OMe	1 h, 4 mol-%	99
15	H	Cl	Cl	1-OMe		27
16	Cl	Cl	H	1-OMe		19

Other substrates:						
	substrate		pre-catalyst	Special Conditions	[%] yield ^[b]	
17	2-bromonaphthalene		1-OMe		98	
18	2-bromofluorene		1-OMe		96	
19	9-bromoanthracene		1-OMe		98	
20	2-bromopyridine		1-OMe		99	
21	benzyl bromide		1-OMe	1 h, 4 mol-%	99	
22	1-bromooctane		1-OMe	1 h, 4 mol-%	98	

[a] Reaction scale: 0.2 mmol of organic halide, 0.016 mmol of Ni catalyst (8 mol-%) (or 0.008 mmol, 4 mol-%, if specified), NaBH₄ (15.0 mg, 0.4 mmol, 2.0 equiv.) and 2 mL dimethylacetamide (DMA), 80 °C 3 h (unless specified).
[b] GC/MS yield, average of three experiments, error ± 3 %.

While detailed experimental and computational analysis of reaction kinetics will be the subject of a future report, some plausible mechanistic pathways can be envisioned based on previous proposals with similar compounds^[16–20] and on the current results. Scheme 2 and Figure S28 give some possible mechanisms. The first step (step A) in any of the paths is the reaction between **1-X** and NaBH₄ to give the (PNN-X)NiH intermediates, **2-X** (X = OMe, Me, CF₃). Given the reported propensity for 1st row transition metals to be involved in single-electron transfer (SET) chemistry, the previous observations of the hemilability of the current ligand, and the observed trends with electronic effects in the catalysis we currently favor the pathway that includes steps A–C, as outlined in the top of Scheme 2. That is, **2-X**, could undergo homolytic cleavage to give (PNN-X)Ni^I, **3-X**, and hydrogen, as hypothesized for other hydridonickel(II) (ZNN) pincer complexes (Z = Ni,^[16,18,19] C^[20]), and as supported by the observation of H₂ in the NMR spectra during reaction monitoring. Such dissociation may be favored for more electron rich ligands as suggested by DFT calculated Ni–H stretching frequencies (1857, 1861, and 1874 cm⁻¹ for **2-OMe**, **2-Me**, and **2-OMe**, respectively). In the ensuing step B, the **3-X** intermediate would presumably undergo oxidative addition



Scheme 2. Potential mechanisms for hydrodehalogenation reactions of organic halides (R-X) catalyzed by [PNN]Ni pincer complexes.

(OA) to aryl halide or 1-bromooctane, by an SET pathway to produce a species with the composition (PNN-X)Ni(R)(Br), **4-X**. Intermediate **4-X**, would likely be tetracoordinated nickel(II) bound to a κ^2 -ligand radical (to give a 16 e-complex) due to internal electron transfer from the ligand to the presumptive highly oxidizing nickel(III) center and pyrazolyl- arm dissociation. This step B would also be favored for more electron rich groups. This latter step rather than step A is thought to be the rate-limiting step given the lack of strong kinetic isotope effect (KIE, vide infra) for reactions involving deuteride, and the variable rates of reaction with changing organohalide or *para*-aryl substituents. In a subsequent step C, NaBH₄ would transfer a hydride to **4-X** to give (PNN-X⁺)Ni^{II}(R)(H), **5-X**. Reductive elimination would give formally a nickel(0) bound to a ligand radical which would immediately reorganize to the nickel(I) pincer, **3-X**. An alternate pathway is possible where (PNN-X)Ni(R), **6-X**, and a bromo radical are produced by OA between **3-X** and organo bromide (perhaps also via dissociation of **4-X**). The bromo radical could abstract a proton from solvent to generate HBr. Any HBr present would then react with (PNN)NiR to give the dehalogenated organic product and (PNN-X)NiBr. Compound **2-X** would be regenerated by reaction with NaBH₄. This alternate mechanism was excluded on the basis of deuterium labeling studies described in the next section. The possibility of a Ni(II)/Ni(0) cycle is described in the Supporting information, but such a cycle does not have literature precedence and the heterolytic cleavage of the Ni–H bond in **2-X** appears less likely than homolytic cleavage.

Several experiments were performed to address the above possibilities. First, it was possible to generate unstable orange-red (PNN-X)NiH intermediates, **2-X**, via the reaction between green **1-X** and either NaBH₄ in THF or NaHBET₃ in THF/benzene mixtures (Supporting Information). The hydrides decompose to small amounts of H₂ gas ($\delta_{\text{H}} = 4.47$ ppm, C₆D₆), free ligand, and

an unidentified brown black paramagnetic species (presumably Ni metal and other species) over the course of a couple hours at room temperature. Freshly prepared samples of **2-X** give characteristic hydride doublet resonances at $\delta_{\text{H}} = -20.6$ ($^2J_{\text{HP}} = 109$ Hz), -20.7 ($^2J_{\text{HP}} = 110.0$ Hz), and -20.9 ($^2J_{\text{HP}} = 112$ Hz) ppm with corresponding doublet ³¹P NMR resonances at $\delta_{\text{P}} = 44.7$, 44.6, 44.1 ppm for **2-OMe**, **2-Me**, and **2-CF₃**, respectively. Appropriately, the ¹H NMR resonances for **2-X** are in between those reported for Liang's [PNP-(*o*-PPh₂C₆H₄)₂N]NiH ($\delta_{\text{H}} = -18.3$ ppm)^[42] and Hu's [NNN]NiH ($\delta_{\text{H}} = -22.8$ ppm).^[16] Moreover, the Ni–H stretch was observed by IR spectroscopy at ν_{NiH} (THF) = 1852, 1853, and 1855 cm⁻¹, for **2-OMe**, **2-Me**, and **2-CF₃**, respectively. These frequencies are similar to Sun's [CNN]NiH ($\nu_{\text{NiH}} = 1894$ cm⁻¹)^[20] derived from compound **D** (Scheme 1) or Lutz's [NNN]NiH (from compound **B**, Scheme 1; $\nu_{\text{NiH}} = 1858$ cm⁻¹)^[18] but higher energy than Hu's [NNN]NiH ($\nu_{\text{NiH}} = 1768$ cm⁻¹).^[16] Next, in the presence of TEMPO, no reaction occurred. This result was not particularly informative as it only indicates that TEMPO reacts irreversibly with a reactive intermediate. Therefore, deuterium-labeling studies were investigated. In the reaction of 4-bromobiphenyl with NaBD₄ and 8 mol-% **1-OMe** (3 h 80 °C) 81 % yield (implying KIE ≥ 1.2 by comparison with Table 3, entry 1) of 4-d₁-biphenyl as the only product, as indicated by its mass spectrum and NMR data. If a solvent-assisted radical pathway were operative one might expect a majority of fully hydrogenated biphenyl. A similar reaction in DMF gave 59 % 4-d₁-biphenyl (implying KIE = 1.3 by comparison with Table 3, entry 19) and 41 % unreacted bromobiphenyl as the only products (Figure S22). The reaction of NaBH₄ in [D₇]DMF neither showed an isotope effect nor gave deuterium incorporation. Thus, the path involving solvent radicals is excluded. Regardless, it is evident that the non-innocence (redox or chemical) of the pincer ligand plays a crucial role in the catalytic activity. The strategy of decorating diarylamido-

based pincer ligands with electron donor groups to improve the hydrodehalogenation activity may be general to nickel pincer complexes of all donor types.

Conclusion

Three new chloronickel(II) complexes of PNN-pincer ligands have been prepared and shown to be excellent pre-catalysts for the hydrodehalogenation of aryl iodides, as well as aryl and alkyl bromides by employing NaBH_4 as a hydride source. The catalytic activity towards aryl chlorides is significantly lower than the bromides but increased with more electron withdrawing substituents in the aryl ring. Deuterium labeling studies demonstrated that NaBH_4 is the sole hydride source, and the involvement of solvent radicals could be excluded. Substitution at the pincer ligand *para*-aniline position with electron donating groups leads to an increase in reactivity due to the increased basicity of the diarylamido nitrogen lone pair. Further substitutions may allow for improvements in activity toward chloro- or fluoro-aromatics, a direction of current study in our group.

Experimental Section

Experimental Details.

Syntheses.

General Considerations.

Chemicals. Solvents for syntheses, spectroscopic characterization or electrochemical studies were dried by conventional means and distilled under Argon prior to use. Solvents used in organic workup or chromatographic separations were used as received from commercial sources. The compound H(PNN) was prepared by the literature method.^[30] All other chemicals were used as received from commercial sources. The new ligands H(PNN-OMe) and H(PNN-CF₃) were prepared according to the procedures outlined in the Supporting Information.

Instrumentation and characterization. Melting point determinations were made on samples contained in glass capillaries using an Electrothermal 9100 apparatus and are uncorrected. Midwest MicroLab, LLC, Indianapolis, Indiana 45250, performed all elemental analyses. ¹H, ¹³C, ¹⁹F, and ³¹P NMR spectra were recorded on either a Varian 300 or 400 MHz spectrometer. Chemical shifts were referenced to solvent resonances at $\delta_{\text{H}} = 7.26$ and $\delta_{\text{C}} = 77.23$ for CDCl_3 or to external references 85 % H_3PO_4 (aq.) $\delta_{\text{P}} = 0$ and 1.0 M $\text{CF}_3\text{CO}_2\text{H}$ in CDCl_3 at $\delta_{\text{F}} = -78.5$ ppm. Electronic absorption (UV/Vis/NIR) measurements were made on a Cary 5000 instrument. Abbreviations for NMR and UV/Vis data: br (broad), sh (shoulder), m (multiplet), ps (pseudo-), s (singlet), d (doublet), t (triplet), q (quartet). FTIR spectra were recorded for either solid samples or THF solutions (KBr plates) in the 4000–500 cm^{-1} region on a Thermo Scientific Nicolet iS5 IR spectrometer equipped with an iD3 Attenuated Total Reflection (ATR) accessory. Electrochemical measurements were collected under a nitrogen atmosphere for samples as 0.1 mM solutions in CH_2Cl_2 with 0.1 M NBu_4PF_6 as the supporting electrolyte. A three-electrode cell comprised of an Ag/AgCl electrode (separated from the reaction medium with a semipermeable polymer membrane filter), a platinum working electrode, and a glassy carbon counter electrode was used for the voltammetric measurements. Data were collected at scan rates of 50, 100, 200, 300, 400, and 500 mV/s. With

this set up, the ferrocene/ferrocenium couple matched the literature value^[43,44] with $E_{1/2} = +0.52$ V in CH_2Cl_2 at a scan rate of 200 mV/s.

Nickel Complexes.

(PNN-OMe)NiCl, 1-Me. A pale green solution of $\text{NiCl}_2 \cdot 6\text{H}_2\text{O}$ (0.237 g, 1.00 mmol) in 4 mL of methanol was added slowly to a magnetically stirred solution of H(PNN-OMe) (0.449 g, 1.00 mmol) in 4 mL of dichloromethane, whereupon the solution immediately became darker green. After 5 min of stirring, a solution of tetraethylammonium hydroxide (0.70 mL of 1.43 M in methanol, 1.0 mmol) was added causing copious green precipitate. After, the resulting dark green suspension had been stirred for 3 h, the green solid was collected by filtration. The filtrate was reduced to 3 mL by rotary evaporation and a second portion of green precipitate was isolated by filtration. The combined green precipitate was rinsed with 3 mL methanol and then was dried under oil pump vacuum (10^{-3} Torr) at room temperature 1 h to give analytically pure **1-OMe** (0.512 mg, yield 94 %) as an olive green powder.

Mp, > 260 °C (dec.). Anal. Calcd. (Found) for $\text{C}_{28}\text{H}_{23}\text{ClN}_3\text{ONiP}$: C, 61.98 (62.12); H, 4.27 (4.27); N, 7.74 (7.50). ¹H NMR (400 MHz, CDCl_3) $\delta_{\text{H}} = 8.12$ (s, 1 H, H₅-pz), 7.99 (s, 1 H, H₃-pz), 7.98 (m, 2 H, *o*-PPh₂^B), 7.87 (m, 2 H, *o*-PPh₂^A), 7.55–7.40 (m, 6 H, *m*- + *p*-PPh₂), 7.34 (d, *J* = 9.0 Hz, 1 H, H₆-tolyl), 7.05–7.01 (m, 3 H, H₄-, H₅-, and H₆-C₆H₄), 6.69 (d, *J* = 2.8 Hz, 1 H, H₃-tolyl), 6.62 (d, *J* = 9.0, 2.8 Hz, 1 H, H₅-tolyl), 6.58 (m, 1 H, H₄-pz), 6.54 (m, H₃-C₆H₄), 3.78 (s, 3 H, OCH₃) ppm. ¹³C NMR (101.52 MHz, CDCl_3) $\delta_{\text{C}} = 162.90$ (d, ²*J*_{C-P} = 26.1 Hz, C₂-C₆H₄), 153.07 (s, C₄-tolyl), 142.89 (s, C₅-pz), 137.61 (s, C₁-tolyl), 133.98 (d, ²*J*_{C-P} = 10.3 Hz, *o*-PPh₂^A), 133.10 (s, C₆-C₆H₄), 132.90 (d, ²*J*_{C-P} = 10.4 Hz, *o*-PPh₂^B), 132.35 (d, ⁴*J*_{C-P} = 1.9 Hz, C₄-C₆H₄), 131.80 (C₂-tolyl), 131.50 (d, ⁴*J*_{C-P} = 2.5 Hz, *p*-PPh₂^A), 131.13 (d, ⁴*J*_{C-P} = 2.4 Hz, *p*-PPh₂^B), 129.45 (d, ¹*J*_{C-P} = 47.1 Hz, *ipso*-PPh₂^B), 129.25 (d, ¹*J*_{C-P} = 59.1 Hz, *ipso*-PPh₂^A), 129.13 (d, ³*J*_{C-P} = 10.7 Hz, *m*-PPh₂^A), 128.70 (d, ³*J*_{C-P} = 11.4 Hz, *m*-PPh₂^B), 128.59 (d, ³*J*_{C-P} = 2.2 Hz, C₃-pz), 123.89 (s, C₆-tolyl), 123.00 (d, ¹*J*_{C-P} = 54.7 Hz, C₁-C₆H₄), 120.63 (d, ³*J*_{C-P} = 11.7 Hz, C₅-C₆H₄), 118.54 (d, ³*J*_{C-P} = 7.3 Hz, C₃-C₆H₄), 114.20 (s, C₅-tolyl), 108.68 (d, ⁴*J*_{C-P} = 1.6 Hz, C₄-pz), 107.94 (s, C₃-tolyl), 56.08 (OCH₃) ppm. ³¹P NMR (162 MHz, CDCl_3) $\delta_{\text{P}} = 30.59$ (s) ppm.

Crystals of **1-OMe** were grown by vapor diffusion of pentane into a solution of 30 mg **1-OMe** in 2 mL C₆H₆.

(PNN-Me)NiCl, 1-Me. In a manner identical to the above, 0.237 g (1.00 mmol) $\text{NiCl}_2 \cdot 6\text{H}_2\text{O}$ in 5 mL of methanol, 0.433 g H(PNN-Me) (1.00 mmol) in 5 mL of dichloromethane, and 0.70 mL of 1.43 M $\text{NEt}_4(\text{OH})$ in methanol (1.0 mmol) gave 0.478 g (91 % yield) **1-Me** as a green powder.

Mp, > 260 °C (dec.). Anal. Calcd. (Found) for $\text{C}_{28}\text{H}_{23}\text{ClN}_3\text{NiP}$: C, 63.86 (63.64); H, 4.40 (4.77); N, 7.80 (8.00). ¹H NMR (400 MHz, CDCl_3) $\delta_{\text{H}} = 8.11$ (s, 1 H, H₅-pz), 8.00 (s, 1 H, H₃-pz), 7.96 (m, 2 H, *o*-PPh₂^B), 7.87 (m, 2 H, *o*-PPh₂^A), 7.55–7.49 (m, 2 H, *p*-PPh₂), 7.49–7.39 (m, 4 H, *m*-PPh₂), 7.34 (d, *J* = 8.5 Hz, 1 H, H₆-tolyl), 7.07– 6.97 (m, 3 H, C₆H₄), 6.96 (s, 1 H, H₃-tolyl), 6.81 (d, *J* = 8.5 Hz, 1 H, H₅-tolyl), 6.57 (br m, 2 H, H₃-C₆H₄ + H₄-pz), 2.25 (s, 3 H, CH₃) ppm. ¹³C NMR (101.52 MHz, CDCl_3) $\delta_{\text{C}} = 162.83$ (d, ²*J*_{C-P} = 25.7 Hz, C₂-C₆H₄), 142.59 (s, C₅-pz), 141.63 (s, C₁-tolyl), 133.98 (d, ²*J*_{C-P} = 10.4 Hz, *o*-PPh₂^A), 133.03 (s, C₆-C₆H₄), 132.87 (d, ²*J*_{C-P} = 10.3 Hz, *o*-PPh₂^B), 132.29 (d, ⁴*J*_{C-P} = 2.1 Hz, *p*-PPh₂^B), 132.15 (d, ⁴*J*_{C-P} = 2.1 Hz, C₄-C₆H₄), 131.22 (C₂-tolyl), 131.12 (d, ⁴*J*_{C-P} = 2.1 Hz, *p*-PPh₂^A), 129.38 (d, ¹*J*_{C-P} = 50.2 Hz, *ipso*-PPh₂^A), 129.26 (d, ¹*J*_{C-P} = 47.0 Hz, *ipso*-PPh₂^B), 129.12 (d, ³*J*_{C-P} = 10.4 Hz, *m*-PPh₂^B), 129.09 (s, C₅-tolyl), 128.91 (s, C₄-tolyl), 128.69 (d, ³*J*_{C-P} = 11.7 Hz, *m*-PPh₂^A), 128.48 (d, ³*J*_{C-P} = 2.1 Hz, C₃-pz), 123.34 (d, ¹*J*_{C-P} = 54.4 Hz, C₁-C₆H₄), 122.75 (s, C₃-tolyl), 122.73 (s, C₆-tolyl), 120.98 (d, ³*J*_{C-P} = 11.7 Hz, C₅-C₆H₄), 118.82 (d, ³*J*_{C-P} = 7.2 Hz, C₃-C₆H₄), 108.48

(d, $^4J_{C-P} = 1.6$ Hz, C₄-pz), 20.84 (CH₃) ppm. ^{31}P NMR (162 MHz, CDCl₃) $\delta_{\text{P}} = 30.32$ (s) ppm. FTIR (cm⁻¹; solid): 3114 (w), 3047 (w), 2863 (w), 1579 (s), 1500 (s), 1456 (s), 1434 (s), 1290 (s).

Crystals of **1-Me** were grown by vapor diffusion of Et₂O into a solution of 30 mg **1-Me** in 3 mL C₆H₆.

(PNN-CF₃)NiCl, 1-CF₃. In a manner identical to the above, 0.237 g (1.00 mmol) NiCl₂·6H₂O in 4 mL of methanol, 0.487 g H(PNN-CF₃) (1.00 mmol) in 4 mL of dichloromethane, and 0.70 mL of 1.43 M NEt₄(OH) in methanol (1.0 mmol) gave 0.541 g (94 % yield) **1-CF₃** as a teal green powder.

Mp, > 260 °C (dec.). Anal. Calcd. (Found) for C₂₈H₂₀ClF₃N₃NiP: C, 57.92 (57.52); H, 3.47 (3.73); N, 7.24 (7.18). ^1H NMR (400 MHz, CDCl₃) $\delta_{\text{H}} = 8.14$ (s, 1 H, H₅-pz), 8.07 (s, 1 H, H₃-pz), 7.95 (dd, $J = 11.4$, 7.9 Hz, 2 H, *o*-PPh₂^B), 7.86 (dd, $J = 12.2$, 7.9 Hz, 2 H, *o*-PPh₂^A), 7.58–7.51 (m, 2 H, *p*-PPh₂), 7.50–7.42 (m, 4 H, *m*-PPh₂), 7.49 (d, $J = 8.4$ Hz, 1 H, H₆-tolyl), 7.39 (s, 1 H, H₃-tolyl), 7.18 (d, $J = 8.4$ Hz, 1 H, H₅-tolyl), 7.15–7.05 (m, 3 H, H₄⁺, H₅⁻, and H₆-C₆H₄), 6.68 (m, 1 H, H₃-C₆H₄), 6.63 (m, 1 H, H₄-pz) ppm. ^{13}C NMR (101.52 MHz, CDCl₃) $\delta_{\text{C}} = 161.94$ (d, $^2J_{C-P} = 24.8$ Hz, C₂-C₆H₄), 143.09 (s, C₅-pz), 148.04 (s, C₁-tolyl), 134.01 (d, $^2J_{C-P} = 10.4$ Hz, *o*-PPh₂^A), 133.17 (s, C₆-C₆H₄), 132.86 (d, $^2J_{C-P} = 10.4$ Hz, *o*-PPh₂^B), 132.63 (d, $^4J_{C-P} = 2.2$ Hz, C₄-C₆H₄), 131.45 (d, $^4J_{C-P} = 3.0$ Hz, *p*-PPh₂^A), 131.42 (d, $^4J_{C-P} = 3.1$ Hz, *p*-PPh₂^B), 130.58 (C₂-tolyl), 129.31 (d, $^3J_{C-P} = 10.7$ Hz, *m*-PPh₂^A), 129.00 (d, $^3J_{C-P} = 1.8$ Hz, C₃-pz), 128.83 (d, $^3J_{C-P} = 11.9$ Hz, *m*-PPh₂^B), 128.66 (d, $^1J_{C-P} = 52.1$ Hz, *ipso*-PPh₂^A), 128.60 (d, $^1J_{C-P} = 48.2$ Hz, *ipso*-PPh₂^B), 124.96 (q, $^3J_{C-F} = 3.3$ Hz, C₅-tolyl), 124.51 (d, $^1J_{C-P} = 53.8$ Hz, C₁-C₆H₄), 122.51 (s, C₆-tolyl), 121.30 (d, $^3J_{C-P} = 11.5$ Hz, C₅-C₆H₄), 122.16 (q, $^1J_{C-F} = 197$ Hz, CF₃), 120.43 (d, $^3J_{C-P} = 7.3$ Hz, C₃-C₆H₄), 120.10 (q, $^2J_{C-F} = 33.6$ Hz, C₄-tolyl), 119.72 (q, $^3J_{C-F} = 4.0$ Hz, C₃-tolyl), 109.12 (d, $^4J_{C-P} = 1.7$ Hz, C₄-pz) ppm. ^{31}P NMR (162 MHz, CDCl₃) $\delta_{\text{P}} = 29.80$ (s) ppm.

Crystals of **1-CF₃** were grown by vapor diffusion of pentane into a solution of 30 mg **1-CF₃** in 2 mL C₆H₆.

Catalysis.

General Procedure. A 100 mL round-bottomed flask equipped with a magnetic stir bar was charged with 0.047 g (0.20 mmol) of 4-bromobiphenyl (or 0.20 mmol of another aryl halide), 8.4 mg (0.016 mmol, 8 mol-%) catalyst **1-X** (or other nickel salt) 15 mg (0.40 mmol, 2.0 equiv.) of NaBH₄ as hydrogen source and 2 mL of dimethylacetamide (DMA) as solvent under argon atmosphere. Next, the magnetically stirred mixture was heated with 80 °C oil bath. After 3 h stirring at 80 °C, the mixture was cooled down and passed through silica gel with rinsing 2 mL of dichloromethane. Then, 1,4-Bis(trimethylsilyl)benzene (11.1 mg) was added as an internal standard and the resulting mixture was subjected to GC-MS for the product analysis. The yields of product and unreacted starting material were also calibrated against standard solutions of biphenyl and 4-bromobiphenyl.

Crystallography. X-ray intensity data from a dark green prism of **1-OMe** (CCDC 2027563), a green plate (P $\bar{1}$, CCDC 2027564) and a green needle (P₂₁/n, CCDC 2027565) of **1-Me**, and a green needle of **1-CF₃** (CCDC 2027566) were collected at 100.0(1) K with an Oxford Diffraction Ltd. Supernova diffractometer equipped with a 135 mm Atlas CCD detector. Mo(K α) radiation was used for the experiments with **1-OMe** and monoclinic **1-Me** while Cu(K α) radiation was used for the other experiments. Raw data frame integration and Lp corrections were performed with CrysAlis Pro (Oxford Diffraction, Ltd.).^[45] Final unit cell parameters were determined by least-squares refinement of 12291, 13164, 10260, and 12849 reflections of **1-OMe**, monoclinic **1-Me**, triclinic **1-Me**, and **1-CF₃**, respectively, with $I > 2\sigma(I)$ for each. Analysis of the data showed negligible crystal

decay during collection in each case. Direct methods structure solutions, difference Fourier calculations and full-matrix least-squares refinements against F^2 were performed with SHELXTL.^[46] Numerical absorption corrections based on Gaussian integration over a multifaceted crystal model were applied to the data in each experiment. All non-hydrogen atoms were refined with anisotropic displacement parameters. Hydrogen atoms were placed in geometrically idealized positions and included as riding atoms. The X-ray crystallographic parameters and further details of data collection and structure refinements are given in Table S1.

Computational Details.

DFT calculations were performed using the Minnesota M06 meta-hybrid GGA functional^[47] because it has been found to be useful for affording accurate solutions to a wide variety of computation problems. Geometry optimizations employed the def2-SV(P) double-zeta basis set^[48] because we previously found^[34,49] (and find again here) that this method provides excellent agreement (within 0.2 Å) with solid-state structures. Solvent (dichloromethane) effects were accounted for by using the polarizable continuum model PCM/UFF,^[50] as implemented in Gaussian 16.^[51] Analytical vibrational frequency calculations were carried out to verify that optimized geometries were stationary points. Time-dependent (TD) DFT methodology^[52–54] was used for excitation energy calculations of the first 25 excited states. Each excitation was fitted to a Gaussian curve with standard deviation of $\sigma = 0.3$ eV and spectra were calculated by summing individual contributions. Tables S4–S7 summarize the results of these studies. Cartesian coordinates are contained within the PNNX_NiCl_DFT.xyz file found in the Supporting Information. Reduction potentials were calculated by using the method outlined by Batista^[55,56] but applying corrections as outlined by Bühl,^[57] where the ultimate potential obtained by $-\Delta G^{\circ}(\text{red, solv} - \text{ox, solv})/F$ was scaled to the Ag/AgCl electrode by subtraction of 4.403 eV (i.e., it was referenced against the absolute SHE potential (CH₂Cl₂) at 4.60 V and then to Ag/AgCl +0.197 V vs. SHE).

Deposition Numbers 2027563, 2027564, 2027565 and 2027566 contain the supplementary crystallographic data for this paper. These data are provided free of charge by the joint Cambridge Crystallographic Data Centre and Fachinformationszentrum Karlsruhe Access Structures service www.ccdc.cam.ac.uk/structures.

Acknowledgments

JRG thanks the donors of the Petroleum Research Fund (#58705-ND3) and Marquette University for support. We thank Brandon Kizer for initial work with syntheses and characterization of **1-Me**.

Keywords: Dehydrohalogenation · Nickel Pincer · PNN ligands · Nickel hydride · Deuterium labelling

- [1] F. Alonso, I. P. Beletskaya, M. Yus, *Chem. Rev.* **2002**, *102*, 4009–4092.
- [2] C. Menini, C. Park, E.-J. Shin, G. Tavoularis, M. A. Keane, *Catal. Today* **2000**, *62*, 355–366.
- [3] G. Chelucci, S. Baldino, G. A. Pinna, G. Pinna, *Curr. Org. Chem.* **2012**, *16*, 2921–2945.
- [4] V. D. Shteingarts, *J. Fluorine Chem.* **2007**, *128*, 797–805.
- [5] M. Hu, Y. Liu, Z. Yao, L. Ma, X. Wang, *Front. Environ. Sci. Eng.* **2017**, *12*, 3.
- [6] J. Ke, H. Wang, L. Zhou, C. Mou, J. Zhang, L. Pan, Y. R. Chi, *Chem. Eur. J.* **2019**, *25*, 6911–6914.
- [7] C. Lei, F. Liang, J. Li, W. Chen, B. Huang, *Chem. Eng. J.* **2019**, *358*, 1054–1064.

- [8] V. Agarwal, Z. D. Miles, J. M. Winter, A. S. Eustáquio, A. A. El Gamal, B. S. Moore, *Chem. Rev.* **2017**, *117*, 5619–5674.
- [9] R. F. Howe, *Appl. Catal. A* **2004**, *271*, 3–11.
- [10] Y. Wang, Y. Wei, W. Song, C. Chen, J. Zhao, *ChemCatChem* **2019**, *11*, 258–268.
- [11] Z.-Z. Zhou, J.-H. Zhao, X.-Y. Gou, X.-M. Chen, Y.-M. Liang, *Org. Chem. Front.* **2019**, *6*, 1649–1654.
- [12] T.-H. Ding, J.-P. Qu, Y.-B. Kang, *Org. Lett.* **2020**, *22*, 3084–3088.
- [13] K. V. Murthy, P. M. Patterson, M. A. Keane, *J. Mol. Catal. A* **2005**, *225*, 149–160.
- [14] A. Scriveranti, B. Vicentini, V. Beghetto, G. Chessa, U. Matteoli, *Inorg. Chem. Commun.* **1998**, *1*, 246–248.
- [15] C. J. E. Davies, M. J. Page, C. E. Ellul, M. F. Mahon, M. K. Whittlesey, *Chem. Commun.* **2010**, *46*, 5151–5153.
- [16] J. Breitenfeld, R. Scopelliti, X. Hu, *Organometallics* **2012**, *31*, 2128–2136.
- [17] M. Weidauer, E. Irran, C. I. Someya, M. Haberberger, S. Enthaler, *J. Organomet. Chem.* **2013**, *729*, 53–59.
- [18] C. Rettenmeier, H. Wadepohl, L. H. Gade, *Chem. Eur. J.* **2014**, *20*, 9657–9665.
- [19] C. A. Rettenmeier, J. Wenz, H. Wadepohl, L. H. Gade, *Inorg. Chem.* **2016**, *55*, 8214–8224.
- [20] Z. Wang, X. Li, H. Sun, O. Fuhr, D. Fenske, *Organometallics* **2018**, *37*, 539–544.
- [21] C. Yao, S. Wang, J. Norton, M. Hammond, *J. Am. Chem. Soc.* **2020**, *142*, 4793–4799.
- [22] R. Shi, Z. Zhang, X. Hu, *Acc. Chem. Res.* **2019**, *52*, 1471–1483.
- [23] Y.-P. Zhang, M. Zhang, X.-R. Chen, C. Lu, D. J. Young, Z.-G. Ren, J.-P. Lang, *Inorg. Chem.* **2020**, *59*, 1038–1045.
- [24] D. Wu, Z.-X. Wang, *Org. Biomol. Chem.* **2014**, *12*, 6414–6424.
- [25] Y. Kim, J. Lee, Y.-H. Son, S.-U. Choi, M. Alam, S. Park, *J. Inorg. Biochem.* **2020**, *205*, 111015.
- [26] S. Das, V. Subramanian, G. Mani, *Inorg. Chem.* **2019**, *58*, 3444–3456.
- [27] X. Yang, Z.-X. Wang, *Organometallics* **2014**, *33*, 5863–5873.
- [28] L.-C. Liang, W.-Y. Lee, Y.-T. Hung, Y.-C. Hsiao, L.-C. Cheng, W.-C. Chen, *Dalton Trans.* **2012**, *41*, 1381–1388.
- [29] C. P. Yap, Y. Y. Chong, T. S. Chwee, W. Y. Fan, *Dalton Trans.* **2018**, *47*, 8483–8488.
- [30] S. Wanniarachchi, J. S. Hewage, S. V. Lindeman, J. R. Gardinier, *Organometallics* **2013**, *32*, 2885–2888.
- [31] B. J. Liddle, R. M. Silva, T. J. Morin, F. P. Macedo, R. Shukla, S. V. Lindeman, J. R. Gardinier, *J. Org. Chem.* **2007**, *72*, 5637–5646.
- [32] L.-C. Liang, P.-S. Chien, J.-M. Lin, M.-H. Huang, Y.-L. Huang, J.-H. Liao, *Organometallics* **2006**, *25*, 1399–1411.
- [33] S. Lapointe, E. Khaskin, R. R. Fayzullin, J. R. Khusnutdinova, *Organometallics* **2019**, *38*, 1581–1594.
- [34] J. S. Hewage, S. Wanniarachchi, T. J. Morin, B. J. Liddle, M. Banaszynski, S. V. Lindeman, B. Bennett, J. R. Gardinier, *Inorg. Chem.* **2014**, *53*, 10070–10084.
- [35] T. J. Morin, S. Wanniarachchi, C. Gwengo, V. Makura, H. M. Tatlock, S. V. Lindeman, B. Bennett, G. J. Long, F. Grandjean, J. R. Gardinier, *Dalton Trans.* **2011**, *40*, 8024–8034.
- [36] L. G. Lavrenova, *Russ. Chem. Bull.* **2018**, *67*, 1142–1152.
- [37] D. L. Reger, J. R. Gardinier, J. D. Elgin, M. D. Smith, D. Hautot, G. J. Long, F. Grandjean, *Inorg. Chem.* **2006**, *45*, 8862–8875.
- [38] C. Hansch, A. Leo, R. W. Taft, *Chem. Rev.* **1991**, *91*, 165–195.
- [39] A. M. Baird, T. A. Davis, M. A. Matthews, *Ind. Eng. Chem. Res.* **2010**, *49*, 9596–9599.
- [40] H. I. Schlesinger, H. C. Brown, A. E. Finholt, J. R. Gilbreath, H. R. Hoekstra, E. K. Hyde, *J. Am. Chem. Soc.* **1953**, *75*, 215–219.
- [41] O. V. Ozerov, C. Guo, L. Fan, B. M. Foxman, *Organometallics* **2004**, *23*, 5573–5580.
- [42] L.-C. Liang, P.-S. Chien, P.-Y. Lee, *Organometallics* **2008**, *27*, 3082–3093.
- [43] D. Bao, B. Millare, W. Xia, B. G. Steyer, A. A. Gerasimenko, A. Ferreira, A. Contreras, V. I. Vullev, *J. Phys. Chem. A* **2009**, *113*, 1259–1267.
- [44] I. Noviandri, K. N. Brown, D. S. Fleming, P. T. Gulyas, P. A. Lay, A. F. Masters, L. Phillips, *J. Phys. Chem. B* **1999**, *103*, 6713–6722.
- [45] *CrysAlisPro*, Agilent Technologies, **2010**.
- [46] G. M. Sheldrick, *Acta Crystallogr., Sect. C* **2015**, *71*, 3–8.
- [47] Y. Zhao, D. G. Truhlar, *Theor. Chem. Acc.* **2008**, *120*, 215–241.
- [48] F. Weigend, R. Ahlrichs, *Phys. Chem. Chem. Phys.* **2005**, *7*, 3297–3305.
- [49] J. R. Gardinier, J. S. Hewage, B. Bennett, D. Wang, S. V. Lindeman, *Organometallics* **2018**, *37*, 989–1000.
- [50] G. Scalmani, M. J. Frisch, *J. Chem. Phys.* **2010**, *132*, 114110.
- [51] M. J. Frisch, G. W. Trucks, H. B. Schlegel, G. E. Scuseria, M. A. Robb, J. R. Cheeseman, G. Scalmani, V. Barone, B. Mennucci, G. A. Petersson, H. Nakatsuji, M. Caricato, X. Li, H. P. Hratchian, A. F. Izmaylov, J. Bloino, G. Zheng, J. L. Sonnenberg, M. Hada, M. Ehara, K. Toyota, R. Fukuda, J. Hasegawa, M. Ishida, T. Nakajima, Y. Honda, O. Kitao, H. Nakai, T. Vreven, J. A. Montgomery Jr., J. E. Peralta, F. Ogliaro, M. Bearpark, J. J. Heyd, E. Brothers, K. N. Kudin, V. N. Staroverov, R. Kobayashi, J. Normand, K. Raghavachari, A. Rendell, J. C. Burant, S. S. Iyengar, J. Tomasi, M. Cossi, N. Rega, J. M. Millam, M. Klene, J. E. Knox, J. B. Cross, V. Bakken, C. Adamo, J. Jaramillo, R. Gomperts, R. E. Stratmann, O. Yazyev, A. J. Austin, R. Cammi, C. Pomelli, J. W. Ochterski, R. L. Martin, K. Morokuma, V. G. Zakrzewski, G. A. Voth, P. Salvador, J. J. Dannenberg, S. Dapprich, A. D. Daniels, Ö. Farkas, J. B. Foresman, J. V. Ortiz, J. Cioslowski, D. J. Fox, *Gaussian 09, Revision C.01, Gaussian, Inc., Wallingford CT*, **2016**.
- [52] G. Scalmani, M. J. Frisch, B. Mennucci, J. Tomasi, R. Cammi, V. Barone, *J. Chem. Phys.* **2006**, *124*, 094107.
- [53] M. E. Casida, C. Jamorski, K. C. Casida, D. R. Salahub, *J. Chem. Phys.* **1998**, *108*, 4439–4449.
- [54] A. D. Laurent, D. Jacquemin, *Int. J. Quantum Chem.* **2013**, *113*, 2019–2039.
- [55] L. E. Roy, E. Jakubikova, M. G. Guthrie, E. R. Batista, *J. Phys. Chem. A* **2009**, *113*, 6745–6750.
- [56] S. J. Konezny, M. D. Doherty, O. R. Luca, R. H. Crabtree, G. L. Soloveichik, V. S. Batista, *J. Phys. Chem. C* **2012**, *116*, 6349–6356.
- [57] L. Castro, M. Bühl, *J. Chem. Theory Comput.* **2014**, *10*, 243–251.

Received: July 29, 2020